Hindawi
Advances in Materials Science and Engineering
Volume 2021, Article ID 6650525, 10 pages
https://doi.org/10.1155/2021/6650525

Research Article

Research on the Prediction Model of the Friction Coefficient of Asphalt Pavement Based on Tire-Pavement Coupling

Miao Yu,[1] **Xinquan Xu**,[2] **Chuanhai Wu**,[2] **Shanqiang Li**,[2] **Mingxia Li**,[1] **and Haifeng Chen**[3]

[1]*National and Regional Engineering Lab for Transportation Construction Materials, College of Civil Engineering, Chongqing Jiaotong University, 66 Xuefu Ave, Nanan District, Chongqing 400074, China*
[2]*Hualu Transport Technology Co.,Ltd., 399 Congyun Road, Baiyun Ave, Baiyun District, Foshan, Guangdong 510420, China*
[3]*Highway and Transportation Management Center of Shaoxing City, Shaoxing 312000, China*

Correspondence should be addressed to Miao Yu; 158163059@qq.com

Received 31 December 2020; Revised 24 January 2021; Accepted 28 January 2021; Published 11 February 2021

Academic Editor: Xu Yang

The correlations between pavement texture and tire pressure with the actual tire-road contact area were first investigated according to the tire-road static contact characteristics; on this basis, the influence mechanisms of speed and pavement texture on the pavement friction coefficient were systematically explored from the angle of tire-road coupling system dynamics via the self-developed dynamic testing system of tire-pavement friction. By integrating the above influence factors, the BP neural network method was applied to the regression of the prediction model for the asphalt pavement friction coefficient. Through the comparison between the model measured value and estimated value, their correlation coefficient R^2 reached 0.73, indicating that this model is of satisfactory prediction accuracy and applicable to the antiskid design of asphalt pavement.

1. Introduction

Pavement skid resistance is closely related to road traffic safety. With good pavement texture as well as hard and wear-resistant aggregates, a pavement will have superior antiskid performance, thus reducing the probability of traffic accidents and increasing traffic safety. The test method and friction mechanism have been investigated frequently in order to accurately evaluate the antiskid performance of asphalt pavements, and on this basis a series of prediction models have been established for the friction coefficient.

1.1. Friction Models Based on Material Properties. In the aspect of friction materials, the corresponding rubber friction models have been proposed by quite a few scholars based on the viscoelasticity of rubber materials. The most representative models among these include the binomial friction model (D.F. Moore) [1] and the fractal friction model (B.N.J. Persson) [2], both of which are established based on the analysis of frictional behaviors, adhesion friction, and lag friction, between rubber on tire tread and the pavement. In addition, R. Savkoor [3] conducted a large number of rubber friction tests under different temperature conditions via the linear friction tester and series friction test system and put forward a phenomenological model considering the relationships among the rubber sliding speed, friction coefficient, and static friction coefficient.

1.2. Friction Models Based on Tire Friction Behaviors. The structural dynamic response of friction behaviors between tire and asphalt pavement cannot be comprehensively characterized by only the rubber frictional characteristics and tire-road static contact characteristics. In the vehicle-pavement coupling system, the tire will undergo obvious geometric shape changes under the actions of internal pressure as well as external pavement counter-forces like shear force, stretching force, and extruding force, rendering the small-deformation hypothesis no longer applicable [4]; moreover, the force analysis of tire-road contact becomes more difficult due to the complicated mechanical properties

of rubber and asphalt pavement. In order to deeply probe the tire-pavement friction mechanism, scholars dedicated to vehicle engineering and road engineering have proposed various evaluation models.

In the field of vehicle engineering, Oden [5] proposed an exponential decaying-type friction model (see (1)) for friction behaviors on the tire-road contact surface through mass measured data, conducted a steady-state analysis and verification of tire-road dynamic contact through the finite element method based on this model, and deemed that this model could characterize the adhesion-sliding friction behaviors after the dynamic tire-road contact. H. C. Zhou and G. L. Wang et al. compared the Coulomb friction model with this model via the finite element method and stated that the tire-road frictional contact model played a decisive role in calculating the maximum braking force. Furthermore, in comparison with the Coulomb friction model, the exponential friction model was closer to the dynamic simulation under the braking condition, and the change law of maximum braking force it embodied was more applicable to the antiskid brake system (ABS) [6]:

$$\mu = \mu_k + (\mu_s + \mu_k)e^{-dc \cdot s}, \tag{1}$$

where μ_k is the dynamic friction factor corresponding to the maximum slip speed, μ_s is the static friction coefficient under critical state, d_c is the pavement condition attenuation coefficient designated by the user, and s is slip speed.

In addition, based on the Grosch rotary-type abrasion machine, Dorsh [7] conducted the friction property test of rubber wheel on dry sandpaper under different load conditions, velocities, and temperatures, proposed the corresponding phenomenological model for the tire friction coefficient, and studied the friction behaviors on the contact surface between the friction model-based tire and smooth pavement via the finite element method. As a function relative to ground pressure intensity, slip speed, and environment temperature, this model can be simply characterized in the form of power exponent as follows:

$$\mu = c_0 p^{c1} v_s^{c2}, \tag{2}$$

where c_0, c_1, and c_2 are all material parameters related to tire-road contact.

Pavement antiskid principles have been explored by many scholars of road engineering, and several classical models commonly applied to the pavement field measurement have been raised [8, 9].

Leu and Henry [10] proposed the Penn State pavement friction coefficient model based on pavement texture and slip speed:

$$\mu = \mu_0 e^{-(S/S_0)}, \tag{3}$$

where μ is the friction coefficient under slip speed S; μ_0 is a constant characterizing the pavement microstructure, dimensionless; and S_0 is a constant characterizing the pavement macrostructure, km/h. A greater μ_0 value represents better pavement microstructure, and a greater S_0 value denotes better pavement macrostructure. According to this model, the pavement friction coefficient is gradually reduced with the increase of speed.

As the average running speed of most vehicles is 60 km/h, the Penn State model is slightly corrected to obtain PIARC model, where two indexes, namely, speed constant S_p and standard friction coefficient F_{60}, are used.

$$\begin{aligned} S_p &= a + b \cdot T_x, \\ F_{60} &= A + B \cdot FR_s \cdot \exp\left[(S - 60)/(a + b \cdot \mathrm{T_x})\right] C \cdot T_x, \end{aligned} \tag{4}$$

where T_x is structural parameter of pavement; a and b are regression coefficients; A, B, and C are system calibration parameters of friction coefficient testing equipment; S is slip speed, km/h; and FR_s is friction coefficient measured under slip speed S. Theoretically speaking, this model can transform the friction coefficient at any test speed into the friction coefficient F_{60} at standard testing speed 60 km/h. However, what is characterized by this model is usually the pavement friction coefficient under full-locked state, and large errors exist in the practical application [11]. In addition, the microtexture has not been fully considered in the above commonly used pavement friction coefficient models, which will influence the prediction accuracy of friction coefficient [12–17]. Though applicable to engineering detection, they are not accurate enough when used in evaluation and research on pavement antiskid performance.

Given this, prediction models for the pavement friction coefficient have not been fully investigated. In order to further reveal the antiskid mechanism of asphalt pavement, (1) the tire-pavement static characteristic test was first implemented based on the principle of tribology and the influences of factors like pavement texture, load, and tire pressure on the actual tire-road contact area were explored. (2) Next, the single-factor analysis was conducted for the influences of factors like slip rate, speed, contact area, and contact pressure intensity on the dynamic tire-road friction behaviors using the self-developed dynamic tire-road friction system. On this basis, an orthogonal test was conducted for ranking the influence degrees of different factors on the dynamic pavement friction coefficient. (3) Based on the above research results, the BP neural network method was combined to establish the prediction model for the dynamic friction coefficient of asphalt pavement. The above research findings are of certain reference values to the prediction of antiskid mechanism and antiskid performance of asphalt pavement.

2. Specimen Fabrication

In view of the major influence of pavement texture on the antiskid performance of asphalt pavement, different types of coarse aggregate-asphalt mixture were selected to prepare slab specimens with the dimensions of $30 \times 30 \times 5$ cm in order to study the influence of macro and microtextures on the antiskid performance of asphalt pavement. Furthermore, gradations originating from the coarse aggregate of basalt, limestone, and granite for asphalt mixtures of AC13, SMA13, and OGFC 13 are shown in Table 1. The asphalt-

Table 1: The gradation of mineral aggregate of asphalt mixtures.

Sieve size (mm)	AC13			SMA13			OGFC13		
	Coarse aggregate types			Coarse aggregate types			Coarse aggregate types		
	Basalt	Limestone	Granite	Basalt	Limestone	Granite	Basalt	Limestone	Granite
16	100	100	100	100	100	100	100	100	100
13.2	97.9	98.5	98.8	96.9	97.7	98.2	96.3	97.2	96.3
9.5	80.5	80.6	80.5	70.6	70.7	69.7	64.3	64.5	64.3
4.75	61.4	60.7	61.6	29.2	28.3	29.9	18.5	17.5	18.5
2.36	44.1	44.5	44.2	24.5	25.8	24.5	10.8	11.7	10.8
1.18	30.6	31.1	30.9	19.1	20.0	19.0	8.2	8.8	8.2
0.6	20.8	21.4	21.1	15.8	16.2	15.5	6.5	6.7	6.5
0.3	14.5	15.1	14.9	13.9	14.1	13.6	5.3	5.3	5.3
0.15	10.1	10.7	10.6	12.6	12.7	12.4	4.4	4.4	4.4
0.075	7.4	7.8	7.8	11.4	11.1	11.0	3.7	3.3	3.7

aggregate ratios of AC13, SMA13, and OGFC13 were 4.8%, 5.0%, and 6.2%, respectively.

3. Methods

3.1. Pavement Texture. 3D texture scanning of the slab specimens was conducted using the linear laser scanning device, with a range of ±10 mm and resolution of ±0.0025 mm. The scanning path is illustrated in Figure 1. Additionally, the macrotextures and microtextures were extracted at different precision levels.

3.1.1. Macrotexture Measurement. In full consideration of macrotexture dimensions and workload during the macrotexture measurement, the sampling interval of the laser profile measuring instrument was adjusted to 0.2 mm, each contour line was 100 mm in length (namely, there were 500 sampling points on each contour line), the spacing of contour lines was 0.2 mm, and 200 contour lines were scanned in a rectangular area 40 mm in width. In this way, a total of 500 × 200 (100,000) points were acquired in each scanning area. On this basis, there were 400,000 points in four areas of one rut slab. It was expected that the calculated macrotext parameters would be representative. The scanning path is seen in Figure 2.

3.1.2. Microtexture Measurement. With reference to the macrotexture scanning direction and accuracy, five coarse aggregates, with particle size of 13.2–16.0 mm and even surfaces, were uniformly selected on the surface of a wheel track tape of each specimen for the microtexture scanning of the aggregate surfaces, where the length of contour line was 1 cm, sampling interval was 5 μm, and 2,000 point elevations were acquired on each contour line. The distance between adjacent contour lines was 1 mm, and six contour lines were scanned, with a total of 12,000 elevation points for every aggregate.

3.2. Static Testing of Tire-Pavement Contact. FUJI pressure film paper with LLW type was pressed on the tire-road contact specimen, and the tire-road static contact test was performed on the TDFA under different pavement textures,

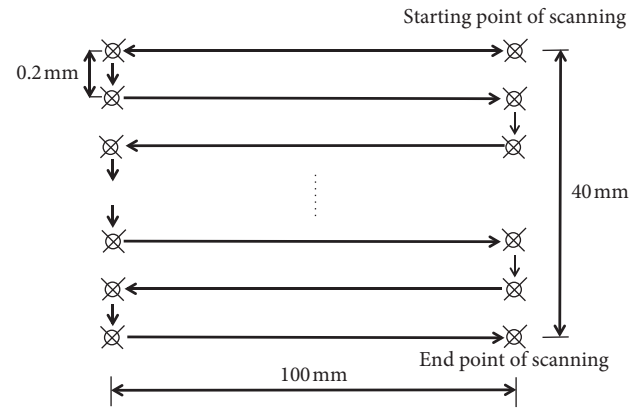

Figure 1: Route laser scanning on the testing.

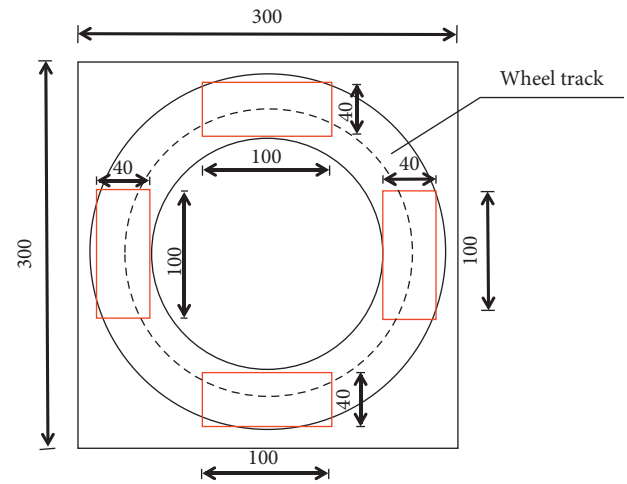

Figure 2: Scanning area on the testing.

upper loads, and tire pressures. More details of TDFA can be found in research by Miao et al. [17]. Furthermore, the tire-road static contact characteristic analysis based on real-time distribution of contact pressure intensity and contact area was carried out with the FPD-8010P pressure film image analysis system. The tire-road static testing conditions are presented in Table 2. The test was repeated three times under each single-factor testing condition.

Table 2: Testing conditions of tire-pavement static contact.

Testing items	Specific parameter range
Pavement textures	0.46, 1.29, 1.41
Tire load (N)	150, 200, 250
Tire pressure (bar)	1.5, 2.0, 2.5, 3.0

Note. The MPD value is obtained from the specimens of AC, SMA, and OGFC by laser scanning.

3.3. Dynamic Testing of Tire/Pavement Friction Coefficient. The dynamic tire-road friction test was implemented on the basis of TDFA. As listed in Table 3, first, the single-factor test of dynamic friction coefficient was conducted based on the running speed and pavement macro-texture, where the test was also repeated three times under each single-factor testing condition.

4. Results and Analysis

4.1. Static Contact Properties of Tire and Pavement

4.1.1. Correlations of Pavement Texture and Upper Load with Actual Contact Area. As shown in Figure 3, the MPD mean values of OGFC, SMA, and AC specimens are 0.46, 1.29, and 1.41, respectively, as seen on the x-coordinate. With the increase of MPD, the actual tire-road contact area is reduced. Although the overall tire-road contact area is significantly enlarged with the increase of upper load, the law "the greater the MPD, the smaller the contact area" remains unchanged.

4.1.2. Correlation between Tire Pressure and Actual Contact Area. The tire-road actual contact areas of nine specimens under different tire pressures were tested, and a further test was implemented in consideration of the tire pressure. As the specimens presented similar laws, only the AC-13 slab specimen with basalt as the coarse aggregate was analyzed in this paper for the investigation of the actual contact area under the coupled impact of tire pressure and upper load.

As shown in Figure 4, it can be inferred that, first, under the same tire load, the tire-road contact area started gradually declining after reaching the maximum value at 2.0 bar with the increase of tire pressure, indicating that when the tire pressure was elevated from 1.5 bar to 2.0 bar, the tire was turned from a "deflated" state into a "blown-up" state, and its contact area with the ground was enlarged; however, with the further air inflation loading, the tire-road contact area was reduced, manifesting that the actual tire-road contact was weakened under unchanged external load with the increase of tire strength. Moreover, under the same tire pressure, the tire-road contact area was apparently enlarged with the increase of tire load, that is, the 150–250 N phase. However, as the tire load was further increased from 250 to 300 N, an increased amplitude of the contact area was not obvious, and even presented flat and declining trends. Furthermore, Figure 5 clearly indicates that as the tire load reached up to 300 N, the width of the tire-road contact zone was enlarged, but the disengaging area in the central zone gradually emerged, indicating that the tire strength was insufficient at the status, and the load-carrying area gradually developed from the crown to side wall of the tire. Based on the above analysis, follow-up research should be conducted within reasonable scopes of tire pressure and load. In subsequent tests, the tire pressure was chosen as 2 bar, 2.5 bar, and 3 bar, and the tire load was chosen as 150 N, 200 N, and 250 N.

Table 3: The single-factor testing conditions of dynamic friction coefficient.

Testing items	Specific parameter range
Slip ratio	20%
Vehicle speed	10 km/h、30 km/h、50 km/h、70 km/h
Macrotexture	The same with Table 2

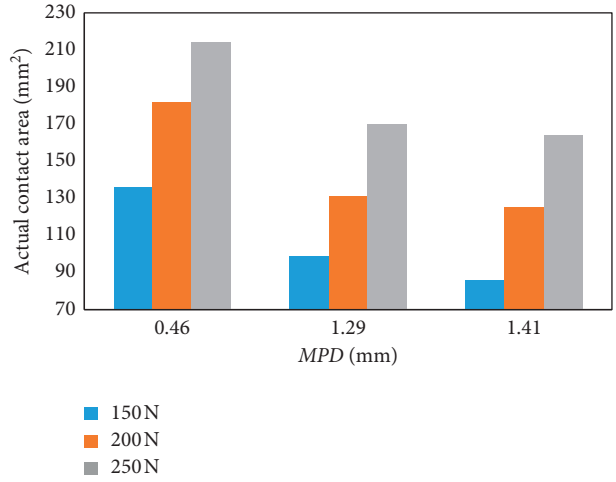

Figure 3: The actual contact area based on different MPD.

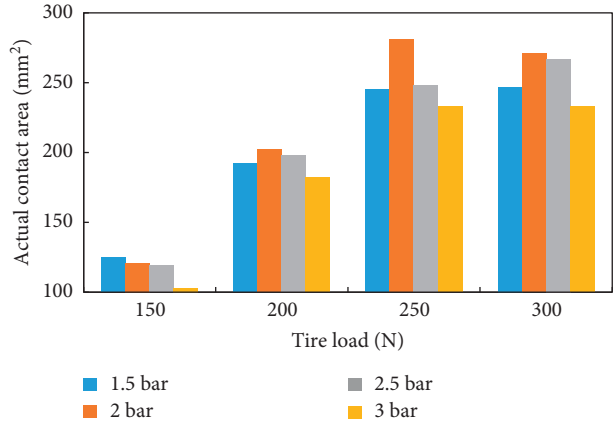

Figure 4: The actual contact area based on different tire loads.

4.2. Dynamically Frictional Properties between Tire and Pavement Based on TDFA

4.2.1. Effect of Tire Speed on Dynamic Friction Coefficient. As shown in Figure 5, the friction coefficients of AC, SMA, and OGFC pavements all presented an obvious declining trend with the increase of vehicle speed. These phenomena

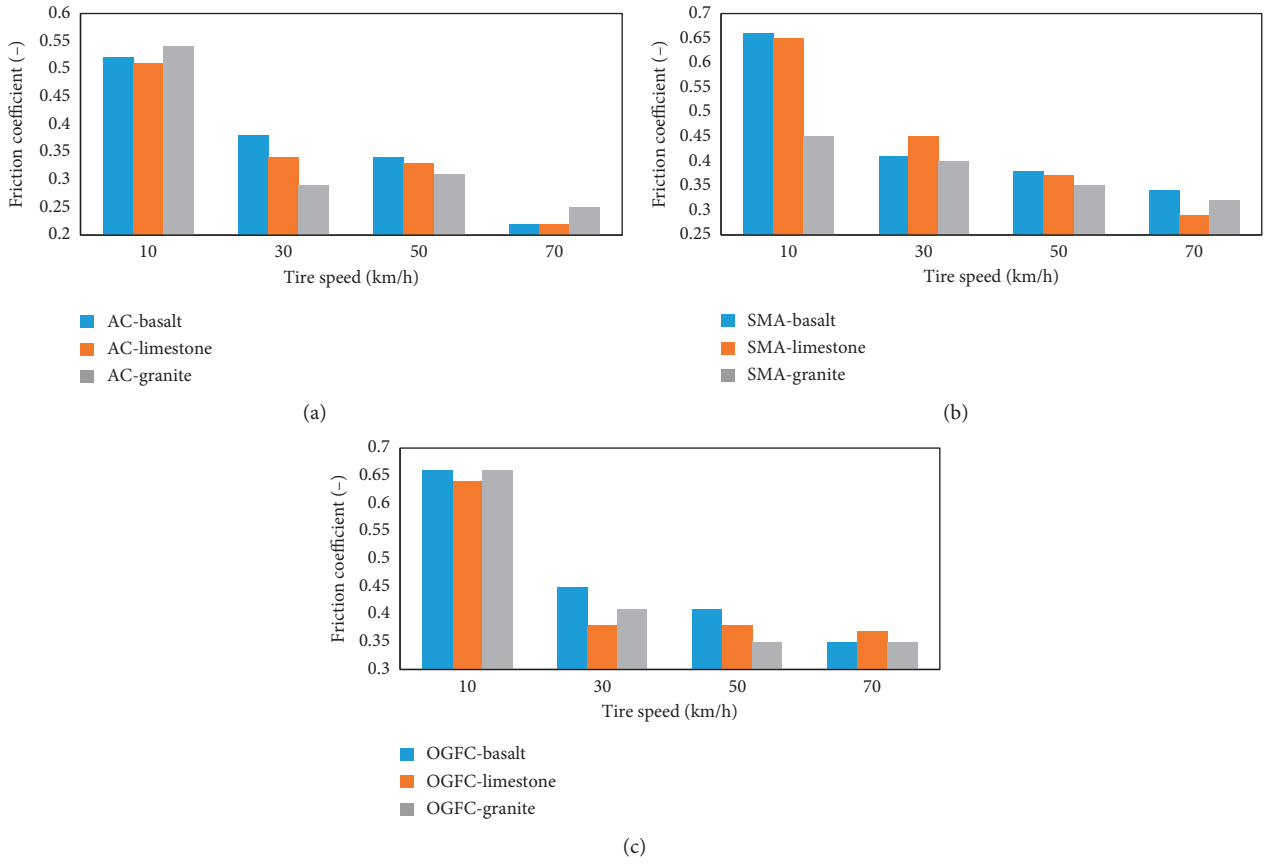

Figure 5: The effect of tire speed on the pavement friction coefficient. (a) The AC pavement friction coefficient under different tire speeds. (b) The SMA pavement friction coefficient under different tire speeds. (c) The OGFC pavement friction coefficient under different tire speeds.

indicate that the acceleration remitted the embedding-squeezing phenomenon between tire and pavement texture, thus leading to the weak tire-pavement adhesion, and, consequently, the effective braking force provided by the pavement to the tire was reduced. In addition, it was found by comparing the different types of pavement that the antiskid performance of OGFC kept the balance with that of SMA, and no obvious advantage of OGFC was found. This can be attributed to the low watering amount during the testing process, so its advantage in keeping good antiskid performance through water drainage was not manifested. In other words, the OFGC could exert its antiskid strength only under large precipitation. By comparing the mixtures with different lithology in the friction coefficient, the antiskid performance of limestone was not significantly different from those of igneous rocks like basalt and granite, indicating that, under the instantaneous braking condition, the abrasion performance of rock had no great impact on its antiskid performance. In the end, the linear regression was conducted for the vehicle speed and friction coefficient on all kinds of pavement, and it was found that the correlation coefficients R^2 of vehicle speed-friction coefficients on AC, SMA, and OGFC pavements were 0.79, 0.64, and 0.53, respectively.

4.2.2. Effect of Pavement Texture on Dynamic Tire-Road Friction Behaviors. It is well known that pavement macrotexture is directly associated with antiskid performance. Furthermore, microtexture also plays a critical role in the antiskid performance, especially the peak value of pavement friction coefficient. The prediction accuracy of pavement antiskid performance can be noticeably improved by incorporating the microtexture into the research on the pavement antiskid performance. Therefore, the aggregate microtextures were characterized using the texture parameter C_{MT}; the physical significance of which was the aspect ratio of microtexture peak, namely, the ratio of altitude difference to horizontal distance of two adjacent points. A greater C_{MT} value represents sharp peaked and rich microtextures. The calculation formula is seen in the following equation, and the calculation results are seen in Table 4:

$$C_{MT} = \frac{1}{n} \frac{\sum_{i=1}^{n} |\Delta h|}{\Delta L}, \tag{5}$$

where C_{MT} is the microtexture coefficient, Δh is the vertical distance between crests of two adjacent microtextures (mm), and ΔL is the horizontal distance between crests of two adjacent microtextures (mm).

Table 4: The microtexture parameter C_{MT} of coarse aggregate.

Coarse aggregate types	Sampling number					Average C_{MT}
	1	2	3	4	5	
Basalt	0.466	0.406	0.424	0.362	0.397	0.411
Limestone	0.450	0.402	0.484	0.387	0.418	0.428
Granite	0.313	0.335	0.379	0.303	0.270	0.320

As seen in Table 4, limestone has the maximum C_{MT} value, followed by basalt and granite, successively, indicating that limestone has the richest microtextures, and the surface of granite is relatively flat with low roughness in this research.

4.2.3. Pavement Friction Coefficient under Multifactor Coupling. The orthogonal test was designed and implemented using the 7-factor and 3-level orthogonal table to further study the influences of pavement texture, load, tire pressure, speed, and so on on the pavement antiskid performance, and the variable designation is listed in Table 5. The macrotextures were controlled via gradation and microtextures controlled using different aggregates. The friction coefficients were tested by TDFA, and four parallel tests were carried out for each group. As the obvious outliers were excluded, the mean value was taken as the test result as seen in the right column of Table 6. The corresponding analysis of variance is displayed in Table 7.

It can be seen from Table 7 that, within the confidence level of 95%, the P value of tire pressure is 0.415, which is greater than 0.05; therefore, it has insignificant influence on the tire-road friction coefficient, whereas the influence levels of the other four factors on the friction coefficient are all 0.00 (smaller than 0.01), indicating extremely significant correlation. Furthermore, by combining the F value ranking, the influence levels of the above factors on the pavement antiskid performance are ranked as macrotexture > speed > microtexture > load.

Table 5: Levels of the variables of the orthogonal test.

Item	Level 1	Level 2	Level 3
Macrotexture (mm)	(A1) 0.46	(A2) 1.29	(A3) 1.41
Tire load (N)	(B1) 150	(B2) 200	(B3) 250
Tire pressure (bar)	(C1) 2	(C2) 2.5	(C3) 3
Tire speed (km/h)	(D1) 10	(D2) 20	(D3) 30
Microtexture (-)	(E1) 0.320	(E2) 0.411	(E3) 0.428

5. Prediction Model Research on Tire-Asphalt Pavement Friction Coefficient

5.1. Modelling for Prediction of the Asphalt Pavement Friction Coefficient Based on BP Neural Network. The BP neural network was used to construct the prediction model for the friction coefficient. The testing samples were selected based on their influence on the pavement friction in the orthogonal test. In consideration of the insignificant correlation of tire pressure with the friction coefficient, the number of input-layer nodes (number of independent variables) was 4 and the number of output-layer nodes (number of dependent variables) was 1 in the neural network after the tire pressure was excluded. On this basis, the number of hidden nodes was finally confirmed as 4 through the cut-and-trial method. There was one input layer in the BP neural network, containing 4 nodes; one hidden layer, containing 4 nodes; and one output layer, containing 1 node, and thus the model solving was realized in the program via the MATLAB programming according to the network structure needed. The steps are as follows.

Step I. The orthogonal test data were saved in the data file to complete the input of sample data. The data were first standardized by converting the input data into numbers within 0–1 to avoid the inaccurate prediction caused by the difference in order of magnitudes, and the processing methods included the max-min method (see (6)) and average number method (see (7)):

$$x_i = \frac{(x_k - x_{\min})}{(x_{\max} - x_{\min})}, \tag{6}$$

where $x_{\min}$ is the minimum data in the input data and $x_{\max}$ is the maximum data in the input data, and

$$x_i = \frac{(x_k - x_{\text{mean}})}{x_{\text{var}}}, \tag{7}$$

where x_{mean} is the mean value of the input data and x_{var} is the variance of the input data.

Step II. The threshold and weight value between layers were randomly initialized according to the determined network structure.

Step III. The neural network was trained according to the standard training process, the weight value and threshold were continuously modified, and the model training was implemented using 80% of the sample number in the program.

Step IV. The network model-based prediction, namely, 20% of the sample data, were reserved in the neural network training to predict model precision and ensure the accuracy of the trained neural network model.

The learning sample data obtained through the test (the comparison chart of sample data training set and test set with the prediction results) were input into the BP neural network, and the equation of factors and friction coefficient were obtained through the MATLAB operation. The

Table 6: The orthogonal test of pavement friction coefficient.

Test no.	Macrotexture	Tire load	Tire pressure	Tire speed	Microtexture	Combination of factors	Friction coefficient
1	A_2	B_2	C_3	D_1	E_3	$A_2B_2C_3D_1E_3$	0.588
2	A_3	B_2	C_2	D_3	E_1	$A_3B_2C_2D_3E_1$	0.488
3	A_2	B_1	C_3	D_3	E_1	$A_2B_1C_3D_3E_1$	0.44
4	A_1	B_2	C_1	D_3	E_3	$A_1B_2C_1D_3E_3$	0.353
5	A_3	B_3	C_3	D_3	E_3	$A_3B_3C_3D_3E_3$	0.536
6	A_2	B_3	C_2	D_1	E_1	$A_2B_3C_2D_1E_1$	0.556
7	A_1	B_3	C_2	D_2	E_3	$A_1B_3C_2D_2E_3$	0.411
8	A_2	B_3	C_1	D_3	E_2	$A_2B_3C_1D_3E_2$	0.491
9	A_2	B_1	C_1	D_2	E_3	$A_2B_1C_1D_2E_3$	0.53
10	A_1	B_1	C_1	D_1	E_1	$A_1B_1C_1D_1E_1$	0.405
11	A_3	B_3	C_1	D_2	E_1	$A_3B_3C_1D_2E_1$	0.546
12	A_3	B_2	C_1	D_1	E_2	$A_3B_2C_1D_1E_2$	0.623
13	A_3	B_1	C_3	D_2	E_2	$A_3B_1C_3D_2E_2$	0.565
14	A_2	B_2	C_2	D_2	E_2	$A_2B_2C_2D_2E_2$	0.541
15	A_1	B_3	C_3	D_1	E_2	$A_1B_3C_3D_1E_2$	0.456
16	A_1	B_2	C_3	D_2	E_1	$A_1B_2C_3D_2E_1$	0.363
17	A_1	B_1	C_2	D_3	E_2	$A_1B_1C_2D_3E_2$	0.34
18	A_3	B_1	C_2	D_1	E_3	$A_3B_1C_2D_1E_3$	0.62

Table 7: ANOVA analysis of the orthogonal test.

Factors	Mean square	F value	P value
Macrotexture	0.058	14261.312	0.000
Tire load	0.001	109.000	0.000
Tire pressure	0.000	1.000	0.415
Tire speed	0.001	4219.750	0.000
Microtexture	0.001	825.062	0.000

coefficients can be seen in Table 8, and the derived equation is seen in the following equation:where x_1 is the macrotexture parameter value (mm), x_2 is the load value (N), x_3 is the speed value (km/h), x_4 is the microtexture parameter value (/), and y is the predicted value of friction coefficient (/).

$$y = \frac{0.1696}{e^a + 1} - \frac{0.0440}{e^b + 1} - \frac{0.1741}{e^c + 1} - \frac{0.1181}{e^d + 1} + 1_{\downarrow},$$

$$a = -5.2989x_1 + 0.0169x_2 + 0.1430x_3 - 22.6687x_4 + g.1314_{\downarrow},$$

$$b = +8.4980x_1 + 0.0223x_2 - 0.1258x_3 + 27.9335x_4 - 16.7806_{\downarrow},$$

$$c = +9.3854x_1 - 0.0051x_2 - 0.0398x_3 + 3.0993x_4 - 12.0751_{\downarrow},$$

$$d = -2.7174x_1 + 0.0192x_2 - 0.1556x_3 - 0.0219x_4 + 3.9483_{\hookleftarrow}. \quad (8)$$

As shown in Figure 6, 80% of the 18 training sample data, namely, 14 data in the training set, were totally consistent with the predicted value of the neural network, the result error was between 20% of the training sample data, namely, 4 data in the test set, and the output value was small, and the absolute error was within 0.05, indicating that the prediction effect of the neural network was accurate, and the neural network model was effective when used to predict the training sample data. To further investigate the validation of the model, the untrained sample data were tested and compared with the measured values.

Table 8: Coefficients used for the predictive model of friction coefficient of asphalt pavement.

		a		b		c		d
X1	–	5.2989	+	8.4980	+	9.3854	–	2.7174
X2	+	0.0169	+	0.0223	–	0.0051	+	0.0192
X3	+	0.1430	–	0.1258	–	0.0398	–	0.1556
X4	–	22.6687	+	27.9335	+	3.0993	–	0.0219
C	+	5.1314	–	16.7806	–	12.0751	+	3.9483
K1	+	0.1696	–	0.0440	–	0.1741	–	0.1181
K2	+				1			

5.2. Model Precision Test. To verify the prediction accuracy of this friction coefficient model, the slab specimens were fabricated for the friction coefficient test. First, the microtexture parameter C_{MT} was calculated after the microtextures on the aggregate surface were scanned, followed by calculation of macrotexture parameter *MPD* after the macrotexture scanning. In the end, the friction coefficients of the slab specimens measured under different operating conditions were compared with the model predicted values to verify the model precision, and the testing conditions, measured values, and predicted values are shown in Table 9.

As presented in Table 8, the data with the absolute value of relative error being smaller than 10% accounted for 45.28%, those with the absolute value of relative error being smaller than 20% accounted for 66.04%, and those with the absolute value of relative error being smaller than 30%

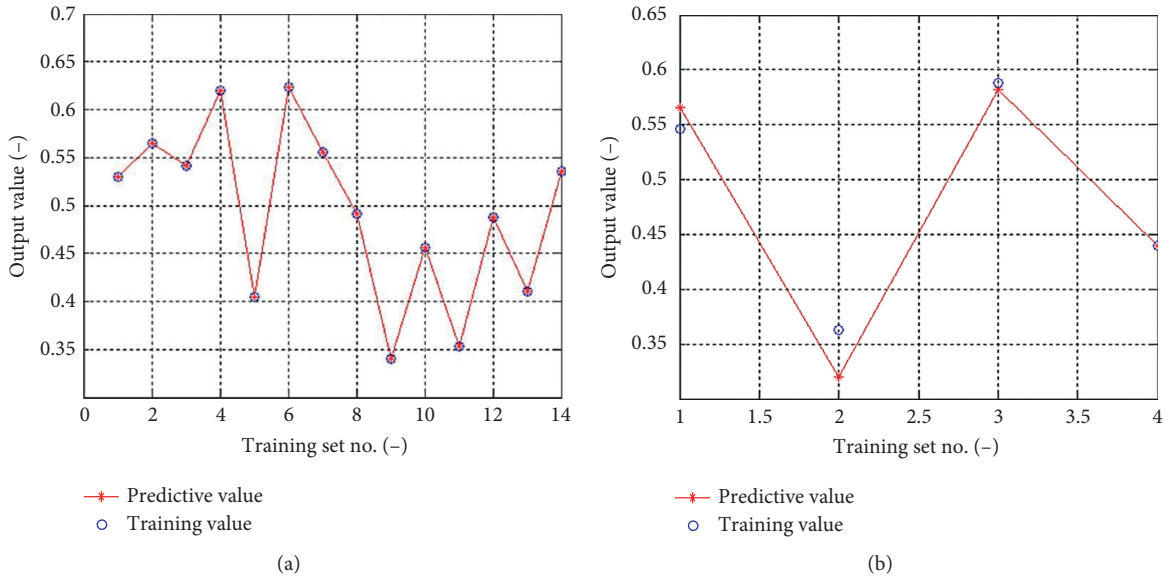

Figure 6: Predictive accuracy of the pavement friction coefficient based on BP neural network. (a) Comparison between the predictive set value and the training set value. (b) Comparison between the predictive set value and the testing set value.

Table 9: The precision test for the predictive model of the pavement friction coefficient.

No.	Macrotexture (mm)	Tire speed (km/h)	Microtexture (mm)	Tire load (N)	Predictive value (/)	Measured value (/)	Error (-)	Relative error (%)
1	0.556	20	0.411	200	0.442	0.41	−0.032	−7.80
2	0.569	20	0.428	200	0.459	0.40	−0.059	−14.75
3	1.293	20	0.320	200	0.521	0.50	−0.021	−4.20
4	1.917	20	0.411	200	0.604	0.61	0.006	0.98
5	1.900	20	0.320	200	0.604	0.53	−0.074	−13.96
6	0.556	10	0.411	200	0.486	0.52	0.034	6.54
7	0.556	30	0.411	200	0.357	0.38	0.023	6.05
8	0.569	10	0.428	200	0.492	0.51	0.018	3.53
9	0.569	30	0.428	200	0.382	0.34	−.0420	−12.35
10	0.556	30	0.320	200	0.287	0.29	0.003	1.03
11	1.609	10	0.411	200	0.654	0.66	0.006	0.92
12	1.353	10	0.428	200	0.606	0.65	0.044	6.77
13	1.353	30	0.428	200	0.502	0.45	−0.052	−11.56
14	1.293	30	0.320	200	0.438	0.40	−0.038	−9.50
15	1.917	10	0.411	200	0.647	0.66	0.013	1.97
16	2.123	10	0.428	200	0.633	0.64	0.007	1.09
17	1.900	10	0.320	200	0.648	0.66	0.012	1.82
18	0.556	20	0.411	250	0.417	0.40	−0.017	−4.25
19	0.569	20	0.428	250	0.437	0.39	−0.047	−12.05
20	0.559	20	0.320	150	0.355	0.32	−0.035	−10.94
21	0.559	20	0.320	250	0.332	0.37	0.038	10.27
22	1.609	20	0.411	250	0.590	0.51	−0.080	−15.69
23	1.353	20	0.428	250	0.570	0.54	−0.030	−5.56
24	1.917	20	0.411	150	0.582	0.55	−0.032	−5.82
25	1.917	20	0.411	250	0.631	0.59	−0.041	−6.95
26	2.123	20	0.428	150	0.574	0.53	−0.044	−8.30
27	2.123	20	0.428	250	0.616	0.61	−0.006	−0.98
28	1.900	20	0.320	150	0.582	0.56	−0.022	−3.93
29	1.900	20	0.320	250	0.631	0.62	−0.011	−1.77
30	0.559	20	0.320	200	0.338	0.47	0.132	28.09
31	1.609	20	0.411	200	0.615	0.46	−0.155	−33.70
32	1.353	20	0.428	200	0.565	0.45	−0.115	−25.56
33	2.123	20	0.428	200	0.590	0.45	−0.140	−31.11
34	0.559	10	0.320	200	0.410	0.54	0.130	24.07

Table 9: Continued.

No.	Macrotexture (mm)	Tire speed (km/h)	Microtexture (mm)	Tire load (N)	Predictive value (/)	Measured value (/)	Error (-)	Relative error (%)
35	1.609	30	0.411	200	0.567	0.41	−0.157	−38.29
36	1.293	10	0.320	200	0.566	0.45	−0.116	−25.78
37	1.917	30	0.411	200	0.572	0.45	−0.122	−27.11
38	1.900	30	0.320	200	0.571	0.41	−0.161	−39.27
39	1.293	20	0.320	250	0.516	0.49	−0.026	−5.31
40	0.556	50	0.411	200	0.204	0.34	0.136	40.00
41	0.556	70	0.411	200	0.176	0.22	0.044	20.00
42	0.569	50	0.428	200	0.209	0.33	0.121	36.67
43	0.569	70	0.428	200	0.176	0.22	0.044	20.00
44	0.559	50	0.320	200	0.196	0.31	0.114	36.77
45	0.559	70	0.320	200	0.175	0.25	0.075	30.00
46	1.609	50	0.411	200	0.508	0.38	−0.128	33.68
47	1.609	70	0.411	200	0.382	0.34	−0.042	−12.35
48	1.353	50	0.428	200	0.395	0.37	−0.025	−6.76
49	1.353	70	0.428	200	0.265	0.29	0.025	8.62
50	1.293	50	0.320	200	0.263	0.35	0.087	24.86
51	1.293	70	0.320	200	0.197	0.32	0.123	38.44
52	1.917	50	0.411	200	0.556	0.41	−0.146	−35.61
53	1.900	70	0.320	200	0.421	0.35	−0.071	−20.26

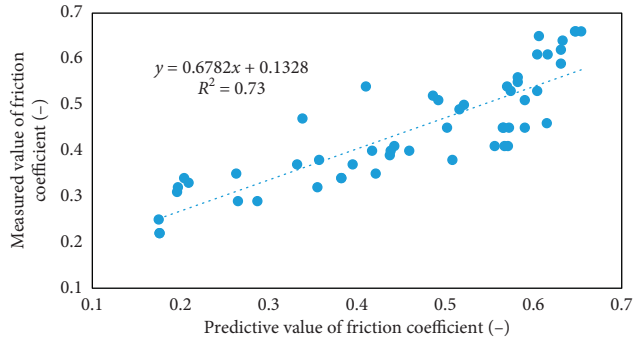

Figure 7: Correlation between the predictive value and the measured value of friction coefficient.

accounted for 81.13%. Additionally, the absolute values of relative errors of all data were within 40%. The correlation between predicted value and measured value of friction coefficient was established as shown in Figure 7 based on Table 8, and their correlation coefficient was obtained as $R^2 = 0.73$, manifesting the favorable model prediction accuracy.

6. Conclusions

The tire-road static contact characteristics were first investigated, the asphalt pavement antiskid performance was tested based on the tire-road coupling friction behaviors, and the prediction model for the asphalt pavement friction coefficient was constructed with the BP neural network in consideration of the pavement macro- and microtexture parameters. The specific conclusions were drawn as follows.

The actual tire-road contact area is reduced with the increase of MPD. However, considering the difference of the pavements with multiple gradations, this conclusion is more applicable for evaluating the relation between the pavements belonging to the same type and friction coefficient.

The ground pressure intensity of tire is increased gradually with the increase of upper load. Nevertheless, it can be known by adding the pressure film scanning analysis that when the upper load is too large, the tire-road ground pressure intensity is gradually migrated from the crown to side wall of the tire. Therefore, the tire pressure should be correspondingly adjusted under different loads to ensure the service life of the tire and driving safety.

As the vehicle speed is accelerated, the friction coefficients of all pavements present a significant declining trend. It was found through the comparison that the OGFC has equivalent antiskid performance to SMA, and no advantage of OGFC is found in the aspect of antiskid performance. It is inferred that no obvious water film is formed on either of the pavements, so the advantage of OGFC in drainage-based skid resistance is not fully embodied. In other words, the OGFC can give full play to its antiskid advantage only under large precipitation.

In comparison with igneous rocks like basalt and granite, the limestone shows no significant difference in the aspect of

instantaneous antiskid performance, indicating that when the aggregates are of favorable angularity, their difference in abrasion performance is not closely related to the antiskid performance.

Based on the orthogonal test of tire-road friction coefficient in full consideration of aggregate texture, tire pressure, speed, and load, the influence degrees of these factors on the asphalt pavement antiskid performance are sorted as macrotexture > speed > microtexture > load.

Based on the influence factors of pavement antiskid performance obtained by the previous conclusion, the BP neural network is added for the regression of the prediction model for the asphalt pavement friction coefficient. The model effectiveness is then verified, and the correlation coefficient R^2 between predicted value and measured value is obtained as 0.73, representing the good prediction accuracy of this model for the friction coefficient.

Data Availability

The underlying data supporting the results of our study are available at http://d.wanfangdata.com.cn/thesis/ChJUaGVzaXNOZXdTMjAyMDEwMjgSCUQwMjAwODI3NxoIZW93czNrMXc%3D.

Conflicts of Interest

The authors declare that they have no conflicts of interest reported in this paper.

Acknowledgments

This work was financially supported by the National Natural Science Foundation of China (no. 51608085), Science and Technology Planning Project of Guangdong Province (no. 2018B020207003), Fundamental Research Funds for the Central Universities, CHD (no. 300102210506), China Postdoctoral Science Foundation (no. 2018M633444), and Shaanxi Province Postdoctoral Science Foundation (no. 2018BSHEDZZ123) awarded to the first author.

References

[1] D. F. Moore, *The Friction and Lubrication of Elastomers*, Pergamon Press, Oxford, USA, 1972.

[2] B. N. J. Persson, "Theory of rubber friction and contact mechanics," *Journal of Chemical Physics*, vol. 115, no. 8, pp. 3840–3861, 2001.

[3] A. R. Savkoor, "Dry adhesive friction of elastomers: A study of the fundamental mechanical aspects," Ph.D. Thesis, Delft University of Technology, Netherlands, 1987.

[4] C. Wei and O. A. Olatunbosun, "Transient dynamic behaviour of finite element tire traversing obstacles with different heights," *Journal of Terramechanics*, vol. 56, pp. 1–16, 2014.

[5] J. T. Oden and J. A. C. Martins, "Models and computational methods for dynamic friction phenomena," *Computer Methods in Applied Mechanics and Engineering*, vol. 52, no. 1-3, pp. 527–634, 1985.

[6] H. Zhou, G. Wang, Y. Ding, J. Yang, and C. L. J. Fu, "Effect of friction model and tire maneuvering on tire-pavement contact stress," *Advances in Materials Science and Engineering*, vol. 2015, Article ID 632647, 2015.

[7] V. Dorsh, A. Becker, and L. Vossen, "Enhanced rubber friction model for finite element simulations of rolling tires," *Plastics. Rubber and Composites*, vol. 31, no. 10, pp. 458–464, 2002.

[8] M. Zheng, H. Zhu, S. Chen et al., "Research progress on anti-sliding performance test and evaluation model for pavement," *Journal of Highway and Transportation Research and Development*, vol. 25, no. 9, pp. 313–318, 2008.

[9] Nchrp 291, "Evaluation of friction characteristics," in *Nchrp Synthesis 291.Transportation Research Board*, National Research Council, Washington D.C., U.S.A., November 2000.

[10] M. C. Leu and J. J. Henry, "Prediction of skid resistance as a function of speed from pavement texture," in *Transportation Research Record 946, Transportation Research Board*, National Research Council, Washington D.C. U.S.A., 1978.

[11] G. Flintsch, E. de L. Izeppi, K. McGhee, and J. Roa, "Evaluation of international friction index coefficients for various devices," in *Transportation Research Record*, Transportation Research Board, January 2008.

[12] S. Aldagari, M. Al-Assi, E. Kassem et al., *Prediction Models for Skid Resistance of Asphalt Pavements and Seal Coat*, Annual Meeting of Transportation Research Board, Washington, D.C., U.S.A., 2018.

[13] N. Zuniga-Garcia, A. de Fortier Smit, and J. A. Prozzi, *Predicting Friction with Improved Texture Characterization*, Annual Meeting of Transportation Research Board, Washington, D.C., U.S.A., 2018.

[14] C. Liu, S. Lv, D. Jin, and F. Qu, "Forthcoming. Laboratory investigation for the road performance of asphalt mixtures modified by rock asphalt/styrene butadiene rubber," *Journal of Materials in Civil Engineering*.

[15] S. Rajaei, K. Chatti, and R. Dargazany, *A Review: Pavement Surface Micro-Texture and Its Contribution To Surface Friction*, Annual Meeting of Transportation Research Board, Washington, D.C., U.S.A., 2017.

[16] Y. Miao, Y. Zhanping, and W. Guoxiong, "Measurement and modeling of skid resistance of asphalt pavement: A review," *Construction and Building Materials*, vol. 260, Article ID 119878, 2020.

[17] Y. Miao, X. Bo, and Y. Zhanping, "Dynamic friction coefficient between tire and compacted asphalt mixtures using tire-pavement dynamic friction analyzer," *Construction and Building Materials*, vol. 258, Article ID 119492, 2020.